ARMY RESEARCH LABORATORY

DFT Study of H_2 Combustion on αAl_2O_3 Supported Pt Clusters

by Jennifer Synowczynski, Jan W. Andzelm, and D. G. Vlachos

ARL-TR-4643 November 2008

NOTICES

Disclaimers

The findings in this report are not to be construed as an official Department of the Army position unless so designated by other authorized documents.

Citation of manufacturer's or trade names does not constitute an official endorsement or approval of the use thereof.

Destroy this report when it is no longer needed. Do not return it to the originator.

Army Research Laboratory
Aberdeen Proving Ground, MD 21005

ARL-TR-4643 **November 2008**

DFT Study of H_2 Combustion on αAl_2O_3 Supported Pt Clusters

Jennifer Synowczynski and Jan W. Andzelm
Weapons and Materials Research Directorate, ARL

and

D. G. Vlachos
University of Delaware

REPORT DOCUMENTATION PAGE

Form Approved
OMB No. 0704-0188

1. REPORT DATE *(DD-MM-YYYY)*	2. REPORT TYPE	3. DATES COVERED (From - To)
November 2008		

4. TITLE AND SUBTITLE
DFT Study of H_2 Combustion on αAl_2O_3 Supported Pt Clusters

5a. CONTRACT NUMBER

5b. GRANT NUMBER

5c. PROGRAM ELEMENT NUMBER

6. AUTHOR(S)
Jennifer Synowczynski, Jan W. Andzelm (ARL), and D. G. Vlachos (University of Delaware)

5d. PROJECT NUMBER

5e. TASK NUMBER

5f. WORK UNIT NUMBER

7. PERFORMING ORGANIZATION NAME(S) AND ADDRESS(ES)
U.S. Army Research Laboratory
ATTN: AMSRD-ARL-MA
Aberdeen Proving Ground, MD 21005

8. PERFORMING ORGANIZATION REPORT NUMBER
ARL-TR-4643

9. SPONSORING/MONITORING AGENCY NAME(S) AND ADDRESS(ES)

10. SPONSOR/MONITOR'S ACRONYM(S)

11. SPONSOR/MONITOR'S REPORT NUMBER(S)

12. DISTRIBUTION/AVAILABILITY STATEMENT
Approved for public release; distribution unlimited.

13. SUPPLEMENTARY NOTES

14. ABSTRACT
Based on Density Functional Theory – Generalized Gradient Approximation (DFT-GGA) calculations, we provide a theoretical model for the hydrogen (H_2) combustion on alumina oxide (Al_2O_3) supported catalytically active platinum (Pt) nanoclusters. In a previous report (Synowczynski, 2008), we identified several adsorption and dissociation processes that occur on the Al_2O_3 support and demonstrated that products from these reactions can migrate along the Al_2O_3 surface. In this report, we build on this model to show how these products influence catalytic activity at the Pt particle. We also identify new reactant structures that are unique to the Pt/Al_2O_3 interface. These processes are key to understanding the "inverse spillover effect" and the influence of the Pt/Al_2O_3 interface during H_2combustion on Al_2O_3 surfaces.

15. SUBJECT TERMS

16. SECURITY CLASSIFICATION OF:			17. LIMITATION OF ABSTRACT	18. NUMBER OF PAGES	19a. NAME OF RESPONSIBLE PERSON
a. REPORT	b. ABSTRACT	c. THIS PAGE	UU	22	Jennifer Synowczynski
U	U	U			19b. TELEPHONE NUMBER (*Include area code*) (410) 306-0750

Standard Form 298 (Rev. 8/98)
Prescribed by ANSI Std. Z39.18

Contents

List of Figures

List of Tables

Acknowledgments

We would like to acknowledge the High Performance Computer (HPC) Modernization program as well as the thoughtful insights of Dr. Eric Wetzel (U.S. Army Research Laboratory), Dr. Emily Carter (Princeton University), and Ioannis Bourmpakis (University of Delaware).

INTENTIONALLY LEFT BLANK.

1. Introduction

As the electronics behind the future warrior systems become more sophisticated, the weight of the batteries is an ever-increasing burden. One solution is to create a compact micro-burner device as shown in figure 1 (Norton et al., 2004) that combusts a higher energy density fuel such as methane (energy density = 3053 W-hr/kg compared to 125 W-hr/kg for lithium (Li)-ion batteries) and converts the released enthalpy into electrical power. The barrier to implementing this technology on the battlefield has been maintaining the flame stability. In confined reactors (i.e., smaller than a few millimeters), the physics is very different from the physics of conventional flames used in macroscopic power generation devices. Flames are unstable due to an increase in both the free radical and thermal quenching at the reactor walls (Miesse, 2004). Both dissipation mechanisms increase in confined systems due to the increase in the surface-to-volume ratio. Maintaining flame stability under these conditions using conventional, homogeneous combustion (flame combustion) requires high operating temperatures (>1000 °C), which are difficult to implement in a compact device. In contrast, catalytic combustion can be performed with high efficiency in sub-millimeter geometries at temperatures as low as 100 °C using a variety of fuels.

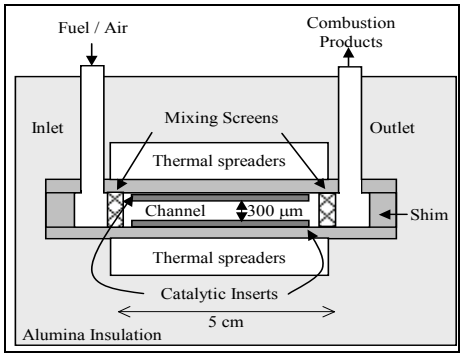

Figure 1. Micro-burner schematic.

Note: The catalytic insert consists of nanosized platinum (Pt) dispersed within porous alumina oxide (Al_2O_3).

Although there are many computational studies which detail the complete reaction mechanism for reactant and product species interacting with the catalytically active cluster, few consider the effect of the Al_2O_3 support. New reaction pathways can arise due to support surface termination. One example of such a pathway is the "inverse spillover effect" (ISE), which occurs when water (H_2O) chemisorbs or dissociates on the support forming mobile species that can migrate to the catalytically active particle and further promote combustion. Experimental evidence for ISE comes from the work of Wang et al. (1996), who demonstrated that carbon monoxide (CO) can liberate hydrogen (H_2) from H_2O bound to Al_2O_3 support. Also of interest is the Pt/Al_2O_3

interface. Theoretical and experimental studies (Ogawa, 1995; Kulawik, 2006; Frondelius, 2008; Hellman, 2008) have shown that charge transfer from the Al_2O_3 support to the metal can induce large structural relaxations at the interface and change the polarity of the metal. In addition, the accumulation of charge on adsorbents such as nitrogen dioxide (NO_2) can create a charge depletion at the oxide-metal interface and subsequently polarize the oxide surface. A complete model of H_2 micro-combustion must encompass all of these effects.

2. Previous Work

In our previous report (Synowczynski, 2008), we performed a theoretical investigation of reaction processes that occurred on the Al_2O_3 support during H_2 combustion. Our model suggested that H_2O is a primary source of mobile oxygen (O) and H species. Although O_2 can adsorb molecularly, it cannot further dissociate to create mobile O. However, H can diffuse away from dissociated water leaving behind an $Al^{[1]}$-OH hydroxyl, which can also further dissociate creating an O•••H pair. The dissociated O•••H pair can diffuse with a barrier ~24 kcal/mol. We also found that H_2 dissociation is an active source of mobile H species.

In this report, we identify the pathways by which these dissociation products diffuse to the Pt particle and participate in catalytically activated H_2 combustion. We also discuss the changes in the alpha-alumina oxide (αAl_2O_3) (0001) surface

3. Model Parameters and Validation

3.1 αAl_2O_3 Surface Termination

Our model (figure 2) consisted of a nine atomic layer thick aluminum (Al)-terminated (0001) slab that is repeated under periodic boundary conditions as a 2x2 supercell with P1 symmetry and a 30Å vacuum layer to prevent any interaction between periodic images. We chose this surface based on the availability of experimental and theoretical data in the literature as well as the work of Marmier et al. (2004), who calculated surface phase diagrams as a function of temperature and the O and H partial pressures for several different crystal orientations and surface terminations. The lattice parameters for the rhombohedral unit cell (a=b= 4.749 Å, c=12.991 Å) were taken directly from experimental results (Swansen, 1960) and were not optimized during the simulation. In addition, we constrained the bottom two layers of the slab to reflect the bulk Al_2O_3 geometry.

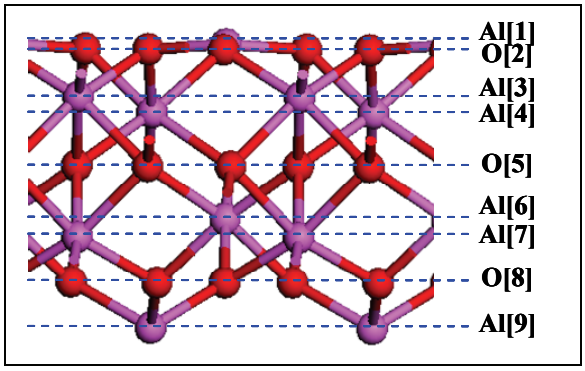

Figure 2. Cross section of fully relaxed Al-terminated αAl_2O_3 (0001) slab used for calculation. O and Al atoms are red and magenta, respectively.

3.2 Model Parameters

All calculations were performed using ideal conditions (0 K, ultra high vacuum, defect free surface). The calculations were executed within the DMol^3 (Delley, 2000) module of the Materials Studio (version 4) software package using a double-numeric basis set with polarization functions (DNP) and the Perdew-Burke-Ernzerhof (PBE) (Perdue, 1996) version of the generalized gradient approximation (GGA) to represent the electron exchange and correlations. The ion cores were described by a density functional semi-core pseudopotential (DSPP) (Delley, 2002).

To validate our calculations, we compare our results for the surface reconstruction of the relaxed αAl_2O_3 (0001) slab with the results of other theoretical and experimental investigations (table 1). In agreement with other theoretical studies, our simulation predicts an 89% contraction of the inter-atomic spacing of top surface layer and 6% expansion of the first sub-layer for the ultra-clean αAl_2O_3 (0001) surface. The predicted surface reconstruction was explained by Sousa et al. (1993) as being a result of charge redistribution due to the highly ionic nature of Al_2O_3. The experimental value for this relaxation is closer to ~50%. The discrepancy between theoretical prediction and experimental measurements may be due to the difficulty in preparing a perfectly terminated surface with no adsorbed atoms or defects.

Table 1. Comparison of theoretical and experimentally measured changes in the inter-atomic layer spacing of Al-terminated αAl_2O_3 (0001) slab with respect to their unrelaxed geometry.

	Theoretical							Experimental	
	Ours	**Hinneman**	**Verdozzi**	**Hass**	**Alavi**	**Ruberto**	**Carrasco**	**Guenard**	**Ahn**
Number of 0xygen layers	3	9	18	3	3	9	11		
Functional	PBE/DSPP	PBE/PAW	LDA/NCPP	PBE/NCPP	PW91/USPP	PW91/NCPP	PBE/PAW		
$Al^{[1]}$-$O^{[2]}$	–89.2	–86.4	–87.4	–98	–97	–85.5	–93.8	–51	63
$O^{[2]}$-$Al^{[3]}$	+6	+4	+3.1	+5	+2	+3.2	+6.1	+16	
$Al^{[3]}$-$Al^{[4]}$	–39.9	–45.4	–41.7	–48	–53	–45.4	–46.7	–29	
$Al^{[4]}$-$O^{[5]}$	+18.9	+20.5	+18.3	+21	–27	+19.8	+22.0	+20	
$O^{[5]}$-$Al^{[6]}$	+17.1	+5	+5.6			+4.8	+8.5		
$Al^{[6]}$-$Al^{[7]}$	–31.2	–6.8	–8.3			–7.1	–11.6		
$Al^{[7]}$-$O^{[8]}$	0	+1.3	+1.1			+1.3	+2.2		
$O^{[8]}$-$Al^{[9]}$	0	–1.3	–0.5			–0.8	+0.7		
$Al^{[9]}$-$Al^{[10]}$		+4.6	+6.4			+3.0	+3.8		
$Al^{[10]}$-$O^{[11]}$		–1.2	–0.6			–0.7	–3.2		

To simulate adsorption phenomena, we added one adsorbate molecule per supercell, which is equivalent to approximately 1/12 monolayer according to Verdozzi et al. (1999), who define a monolayer as having one metal atom per surface oxygen. Binding energies were computed by subtracting the energy of the clean fully relaxed slab and the adsorbent molecule (Pt, H_2O, O_2, H_2) from the total energy of the system after adsorption. We performed barrier calculations for the surface diffusion of O towards the catalytically active Pt particle using the linear synchronous transit (LST) method of Govind et al. (2003) to extrapolate between the reactant and product structures along the diffusion pathways illustrated in figure 3.

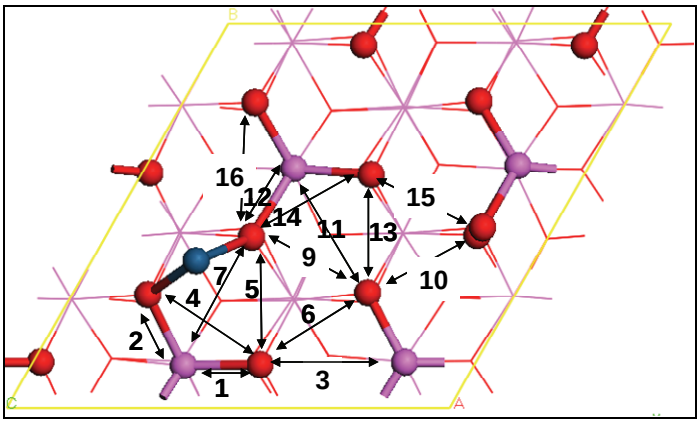

Figure 3. Top view of a 2x2 supercell showing allowed surface binding sites. The Pt position changes slightly for paths 5, 7, 9, 4, 14, and 16 as the diffusing O forms new product structures with Pt. All barrier calculations are performed for O diffusing towards the Pt particle.

Note: The numbers correlate with the product structure and diffusion path notation referred to throughout the report. For Pt product structures the arrow endpoints indicate surface atoms to which Pt binds. For diffusion calculations, the blue atom denotes the position of Pt in the reactant structure and the arrow endpoints refer to the O position in the reactant and product structures.

3.3 Electron Spin State

The reaction chemistry of O involved reactions on Al_2O_3 surfaces cannot be adequately described without careful consideration of the triplet-to-singlet spin conversion that occurs when the $2p\Pi_g^*$ orbitals hybridrize with the surface states. We find the energy difference between the triplet and the singlet ground state of free O_2 to be 19.3 kcal/mol, which is in good agreement with the experimentally measured value of 22.6 kcal/mol (Herzberg, 1950). Figure 4 shows adsorption structures and dissociation products for O, H, O_2, H_2, and H_2O on the Al-terminated αAl_2O_3 (0001) surface. For all adsorption/dissociation products except figure 4A, 4E, and 4J, the lowest energy spin state was singlet. In table 2, we detail the key molecular features for these structures as well as their binding energies. From table 2, it is clear that triplet states result in tighter O=O bonds and a local elongation of the $Al^{[1]}$-O bonding scheme. The spin state has no apparent effect on the length of hydroxyl or $Al^{[1]}$-$H^{[ads]}$ bonds. Based on the binding distances, it would appear that the triplet to singlet spin conversion occurs between 2 and 1.9 Å above the surface for molecular O_2 and between 1.8 and 1.5 Å for atomic O. However, this can only be verified by carefully sampling both the singlet and triplet potential energy surfaces as the adsorbing species approaches the surface.

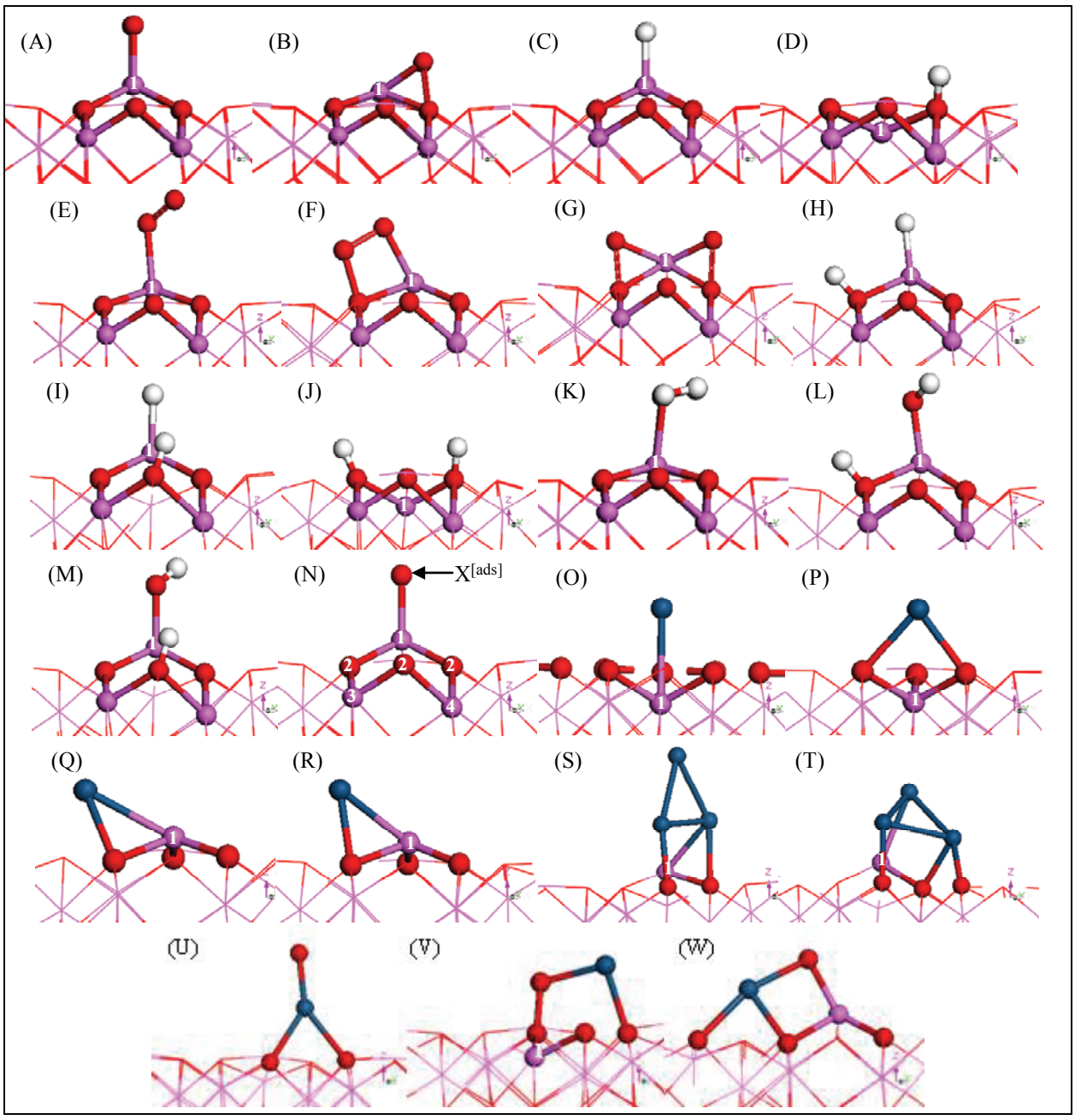

Figure 4. Adsorption and dissociated structures for (A) oxygen tetrahedron, (B) oxygen bridge, (C) hydrogen tetrahedron, (D) hydrogen, (E) 1-1 molecularly adsorbed O_2, (F) 1-2 dissociated O_2, (G) 2-2 dissociated O_2, (H) 1-2 dissociated H_2, (I) 1-4 dissociated H_2, (J) 2-2 dissociated H_2, (K) 1-1 molecularly adsorbed H_2O, (L) 1-2 dissociated H_2O, (M) 1-4 dissociated H_2O, (N) the key indicating atomic layer to which atom originally belonged, (O) Pt directly bound to $Al^{[1]}$, (P) Pt bridging $O^{[2]}$, (Q) Pt bridging $Al^{[1]}$ and $O^{[2]}$, (R) Pt directly bound to $O^{[2]}$, (S) 90° Pt trimer, (T) 37° Pt trimer, (U) O directly bound to the Pt bridge, (V) O bound as a bridge between $O^{[2]}$ and Pt, and (W) O bound as a bridge between $Al^{[1]}$ and Pt.

Note: For structures U, V, W, the Pt atom was in the #10 binding site before relaxation with the adsorbing O atom.

Table 2. Effect of spin state on O_2 adsorption binding energies and bond lengths. The ID notation refers to the structures in figure 4.

Atomic Oxygen Adsorption				
	$E_{binding}$	**$O^{[ads]}$-$O^{[2]}$**	**$O^{[ads]}$-$Al^{[1]}$**	**∠bond**
	(kcal/mol)	**(Å)**	**(Å)**	**(degrees)**
Triplet A	[–42] [a]	–	1.782	112
Singlet A	–30 [–35] [a]	–	1.767	115
Triplet B	[–18] [a]	1.508	1.797	49
Singlet B	–49 [–53] [a]	1.546	1.803	50
Atomic Hydrogen Adsorption				
	$E_{binding}$	**$H^{[ads]}$-$O^{[2]}$**	**$H^{[ads]}$-$Al^{[1]}$**	**∠bond**
Triplet C	–20	–	1.626	114
Singlet C	–36	–	1.625	114
Triplet D	–98	0.971	–	124
Singlet D	–116	0.972	–	124
Molecular Oxygen Adsorption / Dissociation				
	$E_{binding}$	**O=O**	**$O^{[ads]}$-$Al^{[1]}$**	**∠bond**
Triplet E	–7	1.255	1.997	107
Singlet E	–13	1.276	1.959	110
Triplet F	21	1.364	1.895	74
Singlet F	–3	1.393	1.851	76
Triplet G	51	1.499	1.837	48
Singlet G	25	1.522	1.823	49
Molecular Hydrogen Dissociation				
	$E_{binding}$	**$H^{[ads]}$-$O^{[2]}$**	**$H^{[ads]}$-$Al^{[1]}$**	**∠bond**
				OH,HOAl
Triplet H	–15	0.982	1.594	110, 120
Singlet H	–14	0.981	1.593	110, 120
Triplet I	–14	0.971	1.621	120, 113
Singlet I	–10	0.972	1.615	121, 112
Triplet J	–85	0.973	–	127, --
Singlet J	–67	0.973	–	127, --
H_2O Adsorption / Dissociation				
	$E_{binding}$	**$H^{[ads]}$-$O^{[2]}$**	**$O^{[ads]}$-$Al^{[1]}$**	**∠OAlO**
				OH,OAlO
Triplet K	–27 [–23] [b]	0.982	1.982	--, 87
Singlet K	–26 [–23] [b]	0.983	1.987	--, 86
Triplet L	–40 [–33] [b]	0.982	1.740	110, 112
Singlet L	–38 [–33] [b]	0.981	1.740	109, 114
Triplet M	–38 [–33] [b]	0.972	1.759	121, 97
Singlet M	–34 [–33] [b]	0.973	1.758	122, 97

[a]The number in brackets is from Gamallo, 2007
[b]The number in brackets is from Haas, 2000.

Since an objective of this research is to establish how dissociated O from the Al_2O_3 support diffuses to the catalytic particle and all possible surface diffusion pathways include a bridging conformation, we chose to perform our barrier calculations using a singlet spin state for both the reactant and products. This is the most accurate method to explore the effects of crystal symmetry and surface reconstructions on the dissociation and diffusion barriers for reaction

pathways that do not involve a spin change. In future studies, we will perform a detailed sampling of both the triplet and singlet potential energy surfaces using the constrained geometry method to assess the reaction barriers for pathways that involve spin-to-triplet transformations.

4. Results and Discussion

4.1 Adsorption and Dissociation of O, H, O_2, H_2, and H_2O on Al_2O_3 support

Table 3 demonstrates the effect of adsorption and dissociation on the surface reconstruction of the αAl_2O_3 (0001) surface. Although O_2 and H_2O can molecularly adsorb to surface $Al^{[1]}$, H_2 cannot. Molecular O_2 adsorbs closer to the surface than H_2O and does not change the contraction of the first inter-atomic layer. In contrast, molecularly adsorbed H_2O causes the surface $Al^{[1]}$ to contract below the $O^{[2]}$ atoms, changing the surface termination from Al-terminated to O-terminated although the aluminum and oxygen atoms are nearly co-planar.

As shown in figure 4, there are three unique configurations for the dissociated products, henceforth referred to as 1-2, 1-4, and 2-2 dissociation. H_2 can form all three dissociation products; however, H_2O cannot form 2-2 dissociation products and O_2 cannot form 1-4 dissociation products. In comparing the dissociation products, the following trends are clear: (1) dissociation reduces the contraction of the first inter-atomic layer regardless of which species is dissociating and (2) $E_{bind}\, O_2 > E_{bind}\, H_2 > E_{bind}\, H_2O$. In regards to which type of dissociation product has the lowest energy, it depends on which species are present. For both H_2O and O_2, the lowest energy dissociation products are 1-2; however, for H_2, the lowest energy dissociation product is 2-2.

Table3. Effect of adsorption on surface reconstruction.

	Layer1	Layer2	ΔAl[1]	Al[1]-O[2]		
	(%)	(%)	(%)	Å		
Al_2O_3	–89	+6	–	1.704	1.704	1.704
O (A)	–83	+6	+11	1.783	1.783	1.783
O (B)	–98	+9	+8	1.826	1.715	1.714
H (C)	–87	+6	+11	1.784	1.784	1.784
H (D)	Non uniform		–14	1.841	1.747	1.746
O_2 (E)	–90	+7	+7	1.735	1.735	1.733
O_2 (F)	–84	+4	+9	1.878	1.711	1.710
O_2 (G)	–86	+13	+13	1.869	1.862	1.733
H_2 (H)	–83	+10	+13	1.920	1.764	1.764
H_2 (I)	–84	+9	+11	1.796	1.790	1.770
H_2 (J)	Non uniform		–16	1.844	1.837	1.745
H_2O (K)	–104	+6	+6	1.733	1.721	1.720
H_2O (L)	–83	+9	+13	1.894	1.755	1.755
H_2O (M)	–85	+7	+11	1.793	1.779	1.766
Pt (O)	–95	+5	–18	1.810	1.813	1.816
Pt (P)	–87	+6	–17	1.759	1.817	1.826
Pt (Q)	–83	+3	+8	1.710	1.717	1.799
Pt (R)	–92	+6	+9	1.718	1.719	1.828

Note: Layer 1 and Layer 2 are the percent change in the 1st and 2nd inter-atomic layers with respect to their bulk coordinates. A negative sign for Layer 1or 2 represents a contraction of the layer. ΔX[bind] calculates how much the adsorbate pulls the surface $Al^{[1]}$ site from its original relaxed position. $Al^{[1]}$-$O^{[2]}$ are the surface bonds neighboring the adsorption site.

4.2 Adsorption of Pt, Pt-O[ads], Pt_3 on Al_2O_3 Support

Atomic Pt can form four different structures (figure 4O, P, Q, and R) on the αAl_2O_3 (0001) surface, one that is directly bound to $Al^{[1]}$ and three different bridging configurations. The directly bound site has the highest energy site (figure 4O, E_{bind} = -45 kcal/mol). In two of the bridging structures (figure 4Q and R), Pt forms a bridge between $Al^{[1]}$ and $O^{[2]}$ pulling the $Al^{[1]}$ away from the surface; whereas, in the third, Pt bridges two $O^{[2]}$ sites and pushes the nearest $Al^{[1]}$ deeper into the lattice. In general, bridges between $Al^{[1]}$ and $O^{[2]}$ sites have lower energy than bridges between $O^{[2]}$ sites. For the Pt-$O^{[2]}$ bridging structures, the further the adsorption site is from surface and sub-surface Al, the lower the binding energy and the larger the surface bond angle. One interesting point is that all Pt binding configurations change the local surface termination from Al- to O-terminated. This is likely to have a profound effect on catalytic processes. The barrier calculations performed in section 4.3, all contain Pt as a bridging atom in the #10 binding site. For this binding site, we found three unique Pt-$O^{[ads]}$ product structures as illustrated in figure 4U, V, and W.

Pt can also form two different trimer cluster configurations on the αAl2O3 (0001) surface, one that is perfectly perpendicular to the surface ($E_{binding}$ = –79 kcal/mol) and the other that forms a 37° angle ($E_{binding}$ = –94 kcal/mol). Although the surface and internal bonding schemes within

the Pt clusters vary with the sub-surface bonding environment, the binding energies are relatively independent. The Pt-Pt binding distance within the cluster is approximately 2.5 to 2.6 Å. As was the case with atomic Pt, Pt trimer clusters also change the local surface termination from Al- to O-terminated.

Table 4. Effect of the local bonding environment on the binding energies and bond lengths for Pt and Pt trimer product structures. The product structures that result from adsorption at sites 0, (4, 16, 14, 5, 6, 9, 10, 13, 15), (3, 7, 11), and (1, 2, 12) are portrayed in figure 4 as structures O, P, Q, and R, respectively.

Pt Adsorption				
Bind site	**$E_{binding}$**	**$Pt^{[ads]}$-$O^{[2]}$**	**$Pt^{[ads]}$-$Al^{[1]}$**	**∠bond**
0	–45	–	2.571	90
1	–59	2.003	2.422	54
2	–59	2.003	2.420	54
12	–59	2.002	2.422	54
4	–50	2.208	2.700	43
14	–50	2.129	2.716	41
16	–50	2.216	2.703	50
5	–53	2.198	3.092	50
6	–54	2.199	2.996	50
9	–53	2.178	3.093	50
10	–62	2.099	3.638	52
13	–60	3.165	2.091	52
15	–60	3.169	2.099	52
3	–60	2.499	2.067	55
7	–60	2.495	2.067	55
11	–60	2.490	2.057	54
Pt Trimer Adsorption				
	$E_{binding}$	**$Pt^{[ads]}$-$O^{[2]}$**	**$Pt^{[ads]}$-$Al^{[1]}$**	**∠bond**
Figure4S	–79	2.100	2.449	90
Figure4T	–94	2.141	2.527	37

4.3 Surface Diffusion of O Towards a Pt Particle

Table 5 contains the results from the barrier calculations for O surface diffusion towards the catalytically active Pt particle. The presence of Pt decreases the barrier for the diffusion of O in the vicinity of surface $Al^{[1]}$ from 27 kcal/mol to 5 kcal/mol. In addition, it induces an exothermic reaction, which releases 83 kcal/mol of energy by forming a new product with the Pt particle (figure 4W). The energetics for diffusion paths that are > 3.7 Å away from the Pt particle are relatively unaffected by the presence of Pt. This is a preliminary investigation of the effect of surface diffusion and there are still many more pathways and product structures that must be considered before a complete model of O diffusion towards catalytically active Pt particles can be established.

Table 5. Barrier calculations for effect of Pt on O surface diffusion.

	With Pt		No Pt	
Path ID	**$E_{barrier}$**	**E_{rxn}**	**$E_{barrier}$**	**E_{rxn}**
	(kcal/mol)	**(kcal/.mol)**	**(kcal/mol)**	**(kcal/mol)**
14	4.8	–82.5	26.6	0
10	57.8	–1.6	64.4	0
13	61.7	–4.4	64.4	0
15	69.5	+2.8	64.4	0

5. Conclusions

In this report, we identified several adsorption and dissociation products for Pt, Pt-$O^{[ads]}$, Pt_3, O, H, O_2, H_2, and H_2O on the αAl_2O_3 (0001) surface and described how these structures changed the surface reconstruction. Specifically, we concluded that the adsorption of molecular H_2O, atomic Pt, and Pt trimers changed the termination for the αAl_2O_3 (0001) surface from Al- to O-terminated in the vicinity of the adsorption products. This should have a dramatic affect on catalytic activity and surface diffusion. We confirmed this for O surface diffusion near surface $Al^{[1]}$, where the presence of atomic Pt decreased the diffusion barrier from 27 to 5 kcal/mol.

6. References

Ahn, J.; Rabalais, J. W. Composition and Structure of the αAl_2O_3 {0001}-(1x1) Surface. *Surf. Sci.* **1997**, *388*, 121–131.

Alavi, S.; Sorescu, D. C.; Thompson, D. L. Adsorption of HCl on Single-Crystal αAl_2O_3 Surfaces: a DFT Study. *J. Phys. Chem. B* **2003**, *107*, 186–195.

Carrasco, J.; Gomes, J.; Illas, F. Theoretical Study of Bulk and Surface Oxygen and Al Vacancies in αAl_2O_3. *Phys. Rev. B* **2004**, *69*, 064116(1–13).

Delley, B. From Molecules to Solids with the Dmol3 Approach. *J. Chem. Phys.* **2000**, *113*, 7756–7764.

Delley, B. Hardness Conserving Semi-Local Pseudopotentials. *Phys. Rev. B* **2002**, *66*, 155125(1–9).

Elam, J. W.; Nelson, C. E.; Cameron, M. A.; Tolbert, M. A.; George, S. M. Adsorption of H_2O on a Single Crystal αAl_2O_3 (0001) Surface. *J. Phys. Chem. B* **1998**, *102*, 7008–7015.

Guenard, P.; Renaud, G.; Barbier, A.; Gautier-Soyer, M. Determination of αAl_2O_3 (0001) Surface Relaxation and Termination by Measurements of Crystal Truncation Rods. *Surf. Rev. Lett.* **1998**, *5*, 321–324.

Govind, N.; Peterson, M.; Fitzgerald, G.; King-Smith, D.; Andzelm, J. A Generalized Synchronous Transit Method for Transition State Location. *Comp. Mat. Sci.* **2003**, *28*, 250–258.

Hass, K. C.; Schneider, W. F.; Curioni, A.; Andreoni, W. First Principles Molecular Dynamics Simulations of H_2O on αAl_2O_3 (0001). *J. Phys. Chem. B* **2000**, *104*, 5527–5540.

Herzberg, G. *Molecular Spectra and Molecular Structure, I. Spectra of Diatomic Molecules*; Van Nostrand Reinhold Company, New York, 1950.

Hinnemann, B.; Carter, E. Adsorption of Al, O, Hf, Y, Pt and S Atoms on αAl_2O_3 (0001). *J. Phys. Chem. C* **2007**, *111*, 7105–7126.

Marmier, A.; Parker, S. Ab Initio Morphology and Surface Thermodynamics of αAl_2O_3. *Phys. Rev. B* **2004**, *69*, 115409(1–9).

Mhadeshware, A. B.; Vlachos, D. G. A Catalytic Reaction Mechanism for Methane Partial Oxidation at Short Contact Times, Reforming and Combustion, and of Oxygenate Decomposition and Oxidation on Pt. *Ind. Eng. Chem. Res.* **2007**, *46*, 5310–5324.

Norton, D. G.; Voit, K. W.; Bruggemann, T.; Vlachos, D. G. Portable Power Generation via Integrated Catalytic Microcombustion-Thermoelectric Devices. *Proc. 24th Army Science Conference*, 2004.

Perdew, J. P.; Burke, K.; Ernzerhof, M. Generalized Gradient Approximation Made Simple. *Phys. Rev. Lett.* **1996**, *77*, 3865–3866.

Ruberto, C.; Yourdshahyan, T.; Lundqvist, B. Surface Properties of Meta-stable Al_2O_3: a Comparative Study of κ and αAl_2O_3. *Phys. Rev. B* **2003**, *67*, 195412(1–18).

Sousa, C.; Illas, F.; Pacchioni, G. Can Corundum be Described as an Ionic Oxide? *J. Chem. Phys.* **1993**, *99*, 6818–6823.

Swanson, H. E.; Cook, M. I.; Evans, E. H.; de Groot, J. H. Standard X-Ray Diffraction Powder Patter NBS Circular no 539, 10, 3, U.S. Government Printing Office: Washington, DC, 1960.

Synowczynski, J.; Andzelm, J.; Vlachos, D. G. *Theoretical Investigation of H2 Combustion on αAl2O3 Support*; ARL-TR-4642; U.S. Army Research Laboratory: Aberdeen Proving Ground, MD, November 2008.

Verdozzi, C.; Jennison, D.; Schultz, P.; Sears, M. Sapphire (0001) Surface, Clean and with d-Metal Overlayers. *Phys. Rev. Lett.* **1999**, *82*, 799–802.

Wang, D.; Dewaele, O.; Groote, G. F. Reaction Mechanism and Role of the Support in the Partial Oxidation of Methane on Rh/Al_2O_3. *J. Catalysis* **1996**, *159*, 418–426.

No. of Copies	Organization
1 ELEC	ADMNSTR DEFNS TECHL INFO CTR ATTN DTIC OCP 8725 JOHN J KINGMAN RD STE 0944 FT BELVOIR VA 22060-6218
1 HC	DARPA ATTN IXO S WELBY 3701 N FAIRFAX DR ARLINGTON VA 22203-1714
1 CD	OFC OF THE SECY OF DEFNS ATTN ODDRE (R&AT) THE PENTAGON WASHINGTON DC 20301-3080
1 HC	US ARMY TRADOC BATTLE LAB INTEGRATION & TECHL DIRCTRT ATTN ATCD B 10 WHISTLER LANE FT MONROE VA 23651-5850
1 HC	US ARMY INFO SYS ENGRG CMND ATTN AMSEL IE TD F JENIA FT HUACHUCA AZ 85613-5300
1 HC	COMMANDER US ARMY RDECOM ATTN AMSRD AMR W C MCCORKLE 5400 FOWLER RD REDSTONE ARSENAL AL 35898-5000
1 HC	UNIVERSITY OF DELAWARE ATTN D VLACHOS 325 COLBURN LABORATORY NEWARK DE 19716-3110
1 HC	US ARMY RSRCH LAB ATTN AMSRD ARL WM MA J ANDZELM BLDG 4600 RM C204 ABERDEEN PROVING GROUND MD 21005
1 HC	US ARMY RSRCH LAB ATTN AMSRD ARL WM MA J SYNOWCZYNSKI BLDG 4600 RM C219 ABERDEEN PROVING GROUND MD 21005

No. of Copies	Organization
1 HC	US ARMY RSRCH LAB ATTN AMSRD ARL CI OK TP TECHL LIB T LANDFRIED BLDG 4600 ABERDEEN PROVING GROUND MD 21005-5066
3 HC	US ARMY RSRCH LAB ATTN AMSRD ARL CI OK PE TECHL PUB ATTN AMSRD ARL CI OK TL TECHL LIB ATTN IMNE ALC IMS MAIL & RECORDS MGMT ADELPHI MD 20783-1197

Total: 13 (1 Elect, 1 CD, 11 HCs)